

# Clock Synchronization Characterization of the Washington DC Metropolitan Area Quantum Network (DC-QNet)

Wayne McKenzie,<sup>1</sup> Anne Marie Richards,<sup>1</sup> Shirali Patel,<sup>1</sup> Thomas Gerrits,<sup>2</sup> T. G. Akin,<sup>3</sup> Steven Peil,<sup>3</sup> Adam T. Black,<sup>4</sup> David Tulchinsky,<sup>4</sup> Alexander Hastings,<sup>4</sup> Ya-Shian Li-Baboud,<sup>2</sup> Anouar Rahmouni,<sup>2</sup> Ivan A. Burenkov,<sup>5,6</sup> Alan Mink,<sup>7,2</sup> Matthew Diaz,<sup>8</sup> Nijil Lal,<sup>2</sup> Yicheng Shi,<sup>2</sup> Paulina Kuo,<sup>2</sup> Pranish Shrestha,<sup>2</sup> Mheni Merzouki,<sup>9</sup> Alejandro Rodriguez Perez,<sup>10</sup> Eleanya Onuma,<sup>10</sup> Daniel E. Jones,<sup>11,2</sup> Atiyya A. Davis,<sup>12</sup> Thomas A. Searles,<sup>12</sup> J. D. Whalen,<sup>13</sup> Qudsia Sara Quraishi,<sup>14</sup> Kate S. Collins,<sup>15</sup> La Vida Cooper,<sup>10</sup> Harry Shaw,<sup>10</sup> Bruce Crabill,<sup>16</sup> Oliver Slattery,<sup>2</sup> and Abdella Battou<sup>9</sup>

<sup>1</sup>Laboratory for Telecommunication Sciences (LTS), College Park, MD 20740, USA

<sup>2</sup>Information Technology Laboratory, National Institute of Standards and Technology (NIST), Gaithersburg, MD 20899, USA

<sup>3</sup>Clock Development Division, United States Naval Observatory, Washington, DC 20392, USA

<sup>4</sup>Naval Research Laboratory (NRL), Washington DC, 20375, USA

<sup>5</sup>Physical Measurements Laboratory, NIST, Gaithersburg, MD 20899, USA

<sup>6</sup>Joint Quantum Institute and University of Maryland, College Park, MD 20742, USA

<sup>7</sup>Theiss Research, Inc, La Jolla, CA 92037, USA

<sup>8</sup>Dept. of Physics, University of Maryland, College Park, MD 20742, USA

<sup>9</sup>Communications Technology Laboratory, NIST, Gaithersburg, MD 20899, USA

<sup>10</sup>Goddard Space Flight Center, National Aeronautics and Space Administration (NASA), Greenbelt, MD 20771, USA

<sup>11</sup>DEVCOM Army Research Laboratory (ARL), Adelphi, MD 20783, USA

<sup>12</sup>Dept. of Electrical & Computer Engineering, University of Illinois Chicago, IL 60607, USA

<sup>13</sup>Computational Physics Inc., Springfield, VA 22151, USA

<sup>14</sup>ARL, College Park, MD 20742, USA

<sup>15</sup>IREAP, University of Maryland, College Park, MD 20742, USA

<sup>16</sup>Mid-Atlantic Crossroads, College Park, MD 20740, USA

(Dated: 30 September 2024)

Authors to whom correspondence should be addressed: Thomas Gerrits, [thomas.gerrits@nist.gov](mailto:thomas.gerrits@nist.gov); Wayne McKenzie, [wmckenzie@ltsnet.net](mailto:wmckenzie@ltsnet.net)

Quantum networking protocols relying on interference and precise time-of-flight measurements require high-precision clock synchronization. This study describes the design, implementation, and characterization of two optical time transfer methods in a metropolitan-scale quantum networking research testbed. With active electronic stabilization, sub-picosecond time deviation (TDEV) was achieved at integration times between 1 s and  $10^5$  s over 53 km of deployed fiber. Over the same integration periods, 10-picosecond level TDEV was observed using the White Rabbit-Precision Time Protocol (WR-PTP) over 128 km. Measurement methods are described to understand the sources of environmental fluctuations on clock synchronization towards the development of in-situ compensation methods. Path delay gradients, chromatic dispersion, polarization drift, and optical power variations all contributed to clock synchronization errors. The results from this study will inform future work in the development of compensation methods essential for enabling experimental research in developing practical quantum networking protocols.

The potential benefits of quantum networks include theoretically secure quantum key distribution<sup>1</sup>, distributed quantum sensing<sup>2</sup> and computing<sup>3</sup>, and secure clock synchronization<sup>4,5</sup>. High-precision time and frequency synchronization enables fundamental quantum networking capabilities from measuring the indistinguishability<sup>6</sup> of sources to entanglement distribution<sup>7-9</sup> and swapping<sup>10-12</sup>. High-precision clock synchronization is sufficient to support near-term point-to-point quantum communications. As networks scale, the protocol requirements for high-accuracy time synchronization could evolve. Time transfer needs for quantum networking research include the ability to integrate into existing telecommunications infrastructure, co-propagation of quantum and classical signals<sup>13-16</sup>, scalability, resilience,

and security. As single photon pulse durations can vary from nanoseconds to the femtosecond regime using ultrashort lasers, our initial goal is to achieve  $10^{-11}$  s time deviation (TDEV) at one second integration time to enable delivery of entangled photons to distant nodes<sup>17,18</sup>. Optical two-way time and frequency transfer (OTWTF) over fiber can achieve the initial testbed requirements<sup>19-23</sup>. The White Rabbit – Precision Time Protocol (WR-PTP)<sup>24,25</sup> can achieve time and fractional frequency instability of  $10^{-11}$  at one second<sup>26</sup>.

Several groups are currently developing metropolitan-scale quantum networks<sup>23,27-31</sup>. As an emerging testbed to advance research in quantum network metrology and protocols, the Washington DC Metropolitan Quantum Network (DC-QNet)

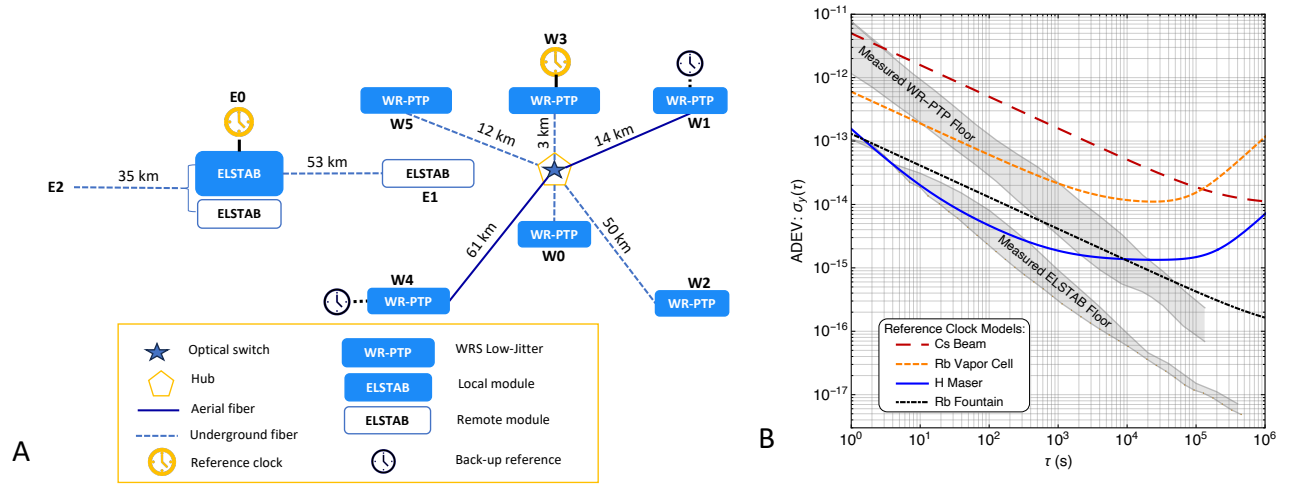


FIG. 1. (A) The electronically stabilized (ELSTAB) and White Rabbit-Precision Time Protocol (WR-PTP) time and frequency transfer methods are deployed as two separate networks in the DC-QNet. E0 through E2 denote the locations of the ELSTAB modules. W0 through W5 denote the locations of the WR-PTP switches. WR-PTP communications pass through the optical switch (links are connected to a point on the star) or are directly connected (links start at a point on the pentagon) at the hub for the tests. (B) Fractional frequency instability models of atomic clocks and optical two-way time and frequency transfer (OTWTFT) methods in the DC-QNet with the measured noise range of the WR-PTP and ELSTAB devices included.

comprises seven locations with deployed underground and aerial optical fibers (Fig. 1A). The DC-QNet integrated and characterized two OTWTFT methods, each with their benefits and limitations. Fig. 1B models the fractional frequency instability of the atomic clocks and the two OTWTFT methods in the DC-QNet. WR-PTP has been employed in various quantum network testbeds ranging from laboratory to metropolitan-scales<sup>13,28,32,33</sup>. Here, we configure White Rabbit Switches (WRS)<sup>34</sup> in a star topology where a centrally located reference clock (W3) synchronizes multiple WRS (Fig. 1A). For each of the links, the WR-PTP time transfer were deployed over two separate fibers operating at identical optical wavelengths, using the dense wavelength division multiplexing (DWDM) either at wavelength 1539.77 nm or at 1541.35 nm. To design and demonstrate a communications network that can co-propagate with quantum signals in the low-loss C-band, we also implemented a single-fiber bi-directional synchronization architecture using coarse wavelength division multiplexing (CWDM) transceivers at 1270 nm and 1290 nm<sup>15</sup>.

A time-correlated single-photon counting (TCSPC) module was used to measure the phase difference between two WRS 10 MHz outputs.

The peak-to-peak phase differences between two WRS were less than 200 ps after subtracting the initial ( $<1$  ns) offset between the two clocks. The Maximum Time Interval Error (MTIE) depicts the peak-to-peak time error observed (Fig. 2A). At averaging intervals  $\leq 10$  s, the MTIE observed over the network was  $< 25$  ps. The Overlapping Allan Deviation (OADEV) between 1 s and  $10^5$  s averaging times was below  $10^{-11}$  (Fig. 2B). The TDEV floor for the underground links dipped below  $10^{-12}$  s at 10 s averaging times (Fig. 2C). Time transfer over aerial links exposed to rapid temperature gradients experienced the most significant instabilities, which was

attributed to time-of-flight fluctuations.

Fig. 2D shows the W3-W4 path delay over the 64 km link as measured by the WRS using 1539.77 nm transceivers based on the time-of-arrival timestamps. This aerial link had an average path delay of 0.32 ms with an average path delay rate of change,  $\frac{\Delta L}{\Delta t} = 1.3$  ps/s, and a maximum path delay rate of change, 21 ps/s, Fig. 2F. The mean one-way path delay of the 53 km W2-W3 underground link (Fig. 2E) is approximately 0.25 ms. In contrast, the average path delay rate of change,  $\frac{\Delta L}{\Delta t}$ , is 0.2 ps/s and the maximum path delay rate of change is 3.5 ps/s. WR-PTP can be used to measure the fiber link delay to adjust transmission for coordinating the time-of-arrival of quantum and classical messages. Aligning the one-way path delay measurements from the WRS at W3 and W4 by time, the delays of the two adjacent fibers remained within 100s of picoseconds. For adjacent fibers, WR-PTP can be employed as a probe signal as these fibers are generally affected by the same changes in delay. The result can be improved by reducing the path delay normalization window. Fig. 2G shows the one-way path delay difference with a normalization window of less than 10 s.

A direct measurement of time-dependent round-trip path delay was performed using optical modulation techniques on both the W3-W2 (53 km) and the E0-E2 (35 km) fiber links. In these measurements, a continuous wave (CW) C-band laser is intensity-modulated at an RF frequency  $f_{\text{mod}}$  using an electro-optic intensity modulator (IM). The bias phase of the IM is actively stabilized using low-frequency feedback to eliminate slow temperature-driven variation in the operating point of the IM. The modulated light propagates through the dark fiber link and is looped back to its origin on a separate fiber strand. The return signal is detected on a photodiode and measured on a lock-in amplifier with reference frequency  $f_{\text{mod}}$  derived from the same signal generator that synthesizes the IM RF in-

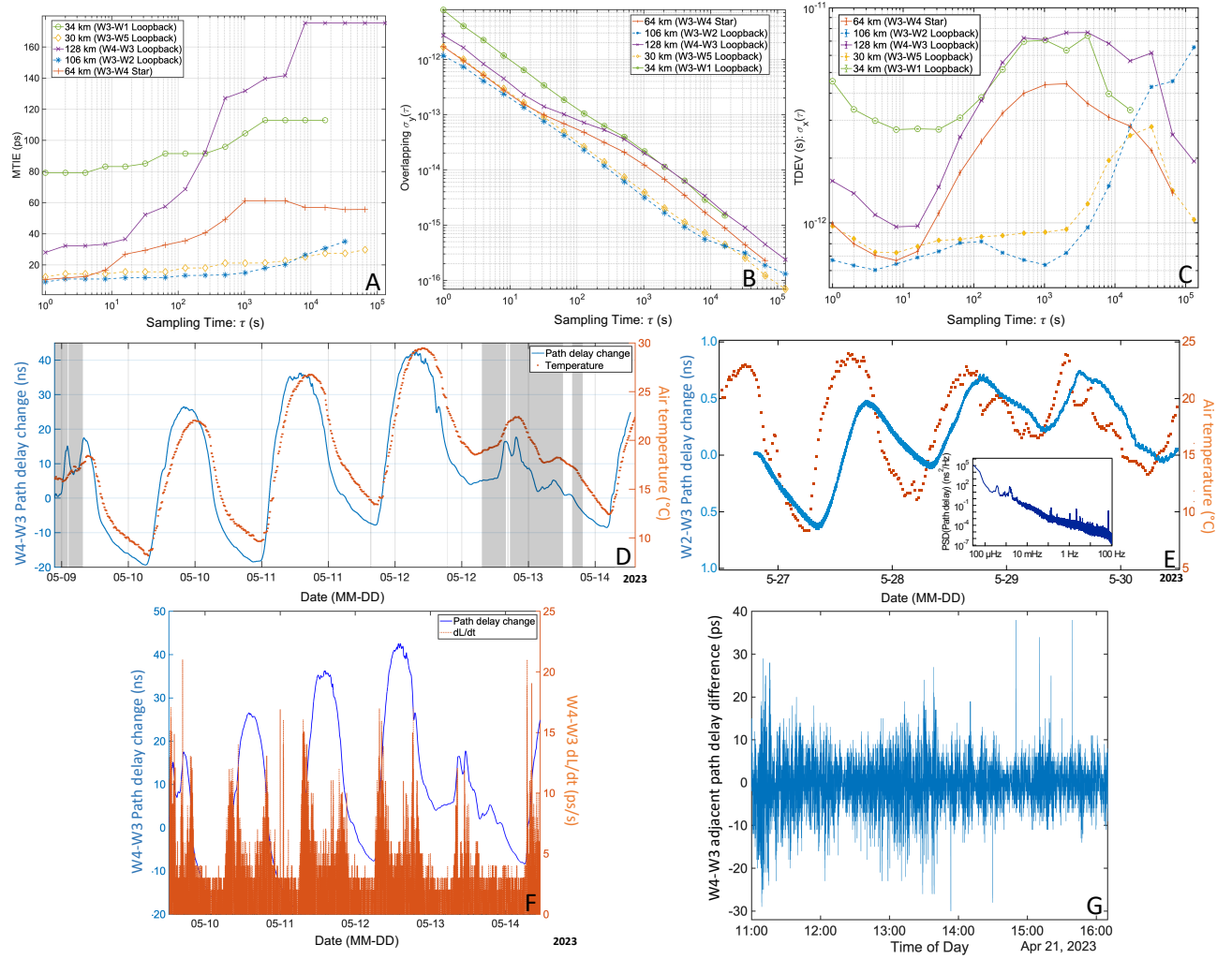


FIG. 2. (A) Maximum Time Interval Error (MTIE) in picoseconds, (B) OADEV, and (C) TDEV for the DC-QNet WR-PTP deployments. The clock errors were measured relative to a reference WRS. (D) One-way path delay of the W4-W3 link (see Fig. 1A) with air temperature measured at a weather station. The shaded areas depict cloud cover. (E) Uncompensated round-trip path delay of the W2-W3 link over a four-day period (solid blue) with temperature measured at a weather station located near W0 (dotted orange). Inset: power spectral density (PSD) of the path delay time trace. (F) One-way path delay (solid blue) and the rate of change (dotted orange) of the W4-W3 link. (G) Differences between the path delay of two adjacent fibers in the same fiber bundle. Both (F) and (G) depict measurements from the W4-W3 aerial fiber.

put. The variation in phase  $\Delta\phi$  of the return-signal modulation relative to the synthesizer phase  $\Delta\tau$  of the total loopback optical link according to  $\Delta\tau = \frac{\Delta\phi}{2\pi f_{\text{mod}}}$ . This method provides high-bandwidth optical path delay measurements in the frequency range from DC to MHz that is independent of the clock distribution architecture. In the 53 km W3-W2 uncompensated path delay measurement (Fig. 2E), the source is a distributed feedback laser at 1547.3 nm. Modulation is provided by an IM driven with  $f_{\text{mod}} = 100$  MHz, and IM bias stabilization is provided by a modulator bias controller. The loopback mean path delay is approximately 0.5 ms as measured separately through a time delay of 100 ns optical pulses. Low-frequency peaks at 0.36 mHz and 1.6 mHz are observed in the power spectrum. The origin of these features is unknown but could be related to

the cycle time of air conditioning in spaces along the fiber path causing high-frequency vibrations and low-frequency temperature variations<sup>35</sup>.

The electronically stabilized (ELSTAB) OTWTF<sup>36-40</sup> deployed in the DC-QNet (Fig. 1A) employs a commercial<sup>37</sup> system with a Local module (E0) used to transfer a stable radio frequency (RF) (usually 10 MHz) and 1 pulse-per-second (PPS) signals to a Remote module. The clock outputs of the Remote module can generally achieve a fractional frequency instability of  $10^{-13}$  at one second, which integrates as white phase noise ( $1/\tau$ ).

Two pairs of RF over fiber modules transmit and receive the 10 MHz and 1 PPS signals, at distances of 53 km (E0-E1) and 70 km (E0-E2 loopback), referenced to a Coordinated Uni-

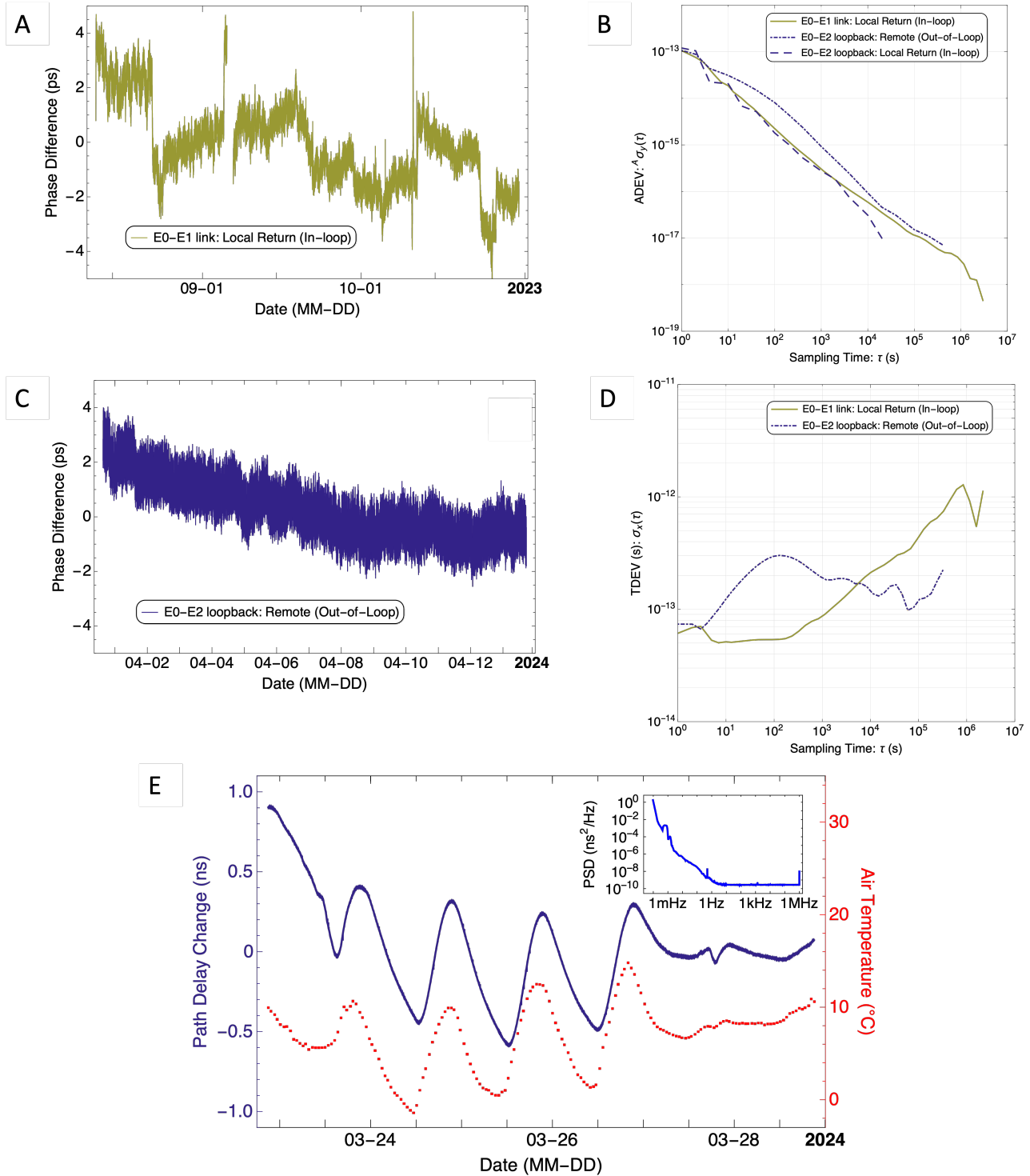


FIG. 3. Phase difference plots between a 10 MHz signal transmitted via ELSTAB on a fiber link and the reference for that transmission. (A) The transmission occurs over a 53 km link. Due to operation constraints, the measurement is made using the “Return” output of the Local module. (B) ADEV for links between E0 and E1 (Blue), E2 (Green). (C) The transmission is on a 35 km link. The loopback installed on this link allows for direct measurement of the reference versus the output of the Remote module. (D) TDEV of the same links. (E) Uncompensated round-trip path delay of the 35 km underground link over a six-day period (blue) and temperature measured at a weather station near E2 (red). Inset: power spectral density of the path delay time trace.

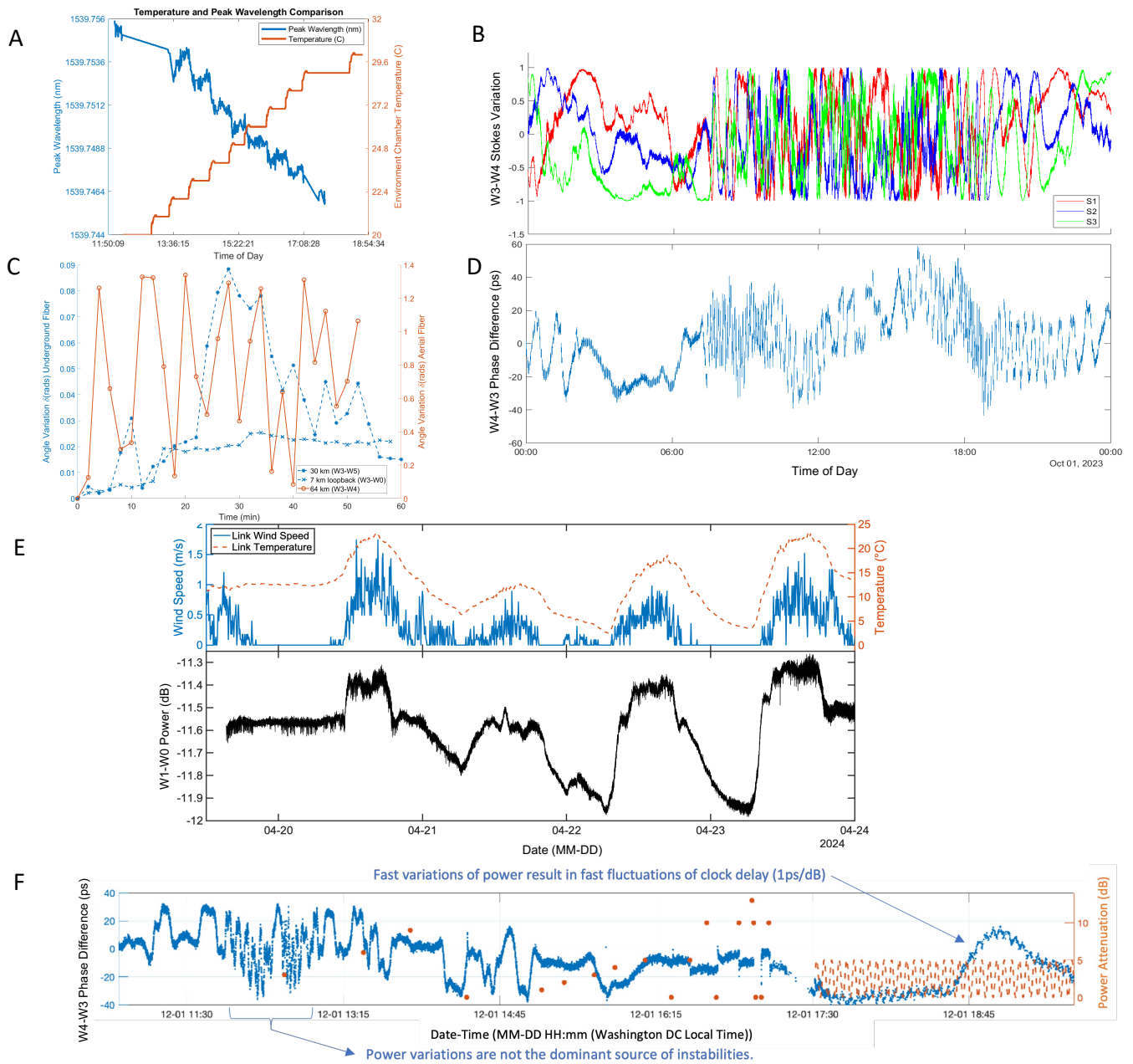


FIG. 4. Characterization of clock transfer links. (A) Wavelength variation of the small form-factor pluggable (SFP) source when placed in an incubator at controlled temperatures. (B) Stokes vector variation over the course of 24 hours on the W3-W4 link. (C) State of polarization (SOP) angle variation of the W3-W5 and W3-W0 loopbacks, taken on different days for one hour from 12:00 PM-1:00 PM local time. The W3-W4 link is also included (aerial fiber). (D) The phase differences between the WR 10 MHz clocks exhibit diurnal variations with improved stability at night (Fig. 1A). (E) The variation in wind speed and temperature (top) in comparison to the optical power (bottom) fluctuations over a primarily aerial 14 km W1-W0 link. (F) Clock phase differences while varying power attenuation at W4.

versal Time (UTC)-traceable ensemble of atomic clocks<sup>41,42</sup>. The relative phase measurement was taken between the reference input and the clock outputs. To maintain continuous operation, the E0-E1 OTWTFT characterization is limited to non-invasive measurements. We compared the RF return against the RF input. Fig. 3A shows the “in-loop” phase difference measurements between the two signals over several months. The  $\sim 12$  hour break in data on 5 September was a

temporary drop in the local data collection. Nonetheless, the OTWTFT over the E0-E1 link maintained uninterrupted operation. To determine the Remote clock’s performance, local access is required. The out-of-loop performance of the ELSTAB method was measured using a loopback configuration on a pair of fibers connecting E0 and E2. With co-located Local and Remote modules, a measurement was performed comparing the Remote output against the 10 MHz signal input on a

70 km (roundtrip) deployed link: Fig. 3B shows nearly two weeks of phase difference. Throughout the data collection period, the phase difference remained within 10 ps, consistent in both links. Fig. 3C displays the ADEV for the measurements. The Remote output on the E0-E2 link performs as well as the Local return output on the E0-E1 link for averaging times less than 10 s. For longer averaging times, the Remote output appears to accumulate some additional noise not measured in the Local return output. Without access to the internal components of the Local or Remote modules, we can only speculate on the source of the noise (e.g., competition from multiple reflections at poor splices or connections or electronic noise in the Remote module that is external to the interferometer path). Fig. 3D shows the corresponding TDEV for the two measurements, which meets the anticipated stability requirements for near-term protocols relying on quantum interference. For the E0-E2 path delay measurement, Fig. 3E shows the change in phase record over a six day period. The mean path delay of 338  $\mu$ s was determined from an independent, time-interval measurement of a 1PPS signal transmitted on the link. Similar to Fig. 2D, a strong correlation is evident between the path delay and the air temperature gradients for both Fig. 2E and Fig. 3E. However a much smaller path delay amplitude is observed, as is a time delay of  $\sim 3$  hour in the response of fiber path delay to temperature changes. The lag between delay and temperature change suggests that most of the fibers for both links are underground.

There is a link delay asymmetry due to different group delays from the 1.6 nm wavelength separation between the WR-PTP bi-directional upstream and downstream communications. In addition, there are temperature-dependent wavelength fluctuations caused by chromatic dispersion. The emitted SFP output wavelength was measured using an optical spectrum analyzer (OSA) over the deployed fiber (Fig. 4A). The switches were placed in an incubator where the temperature increased 1°C every 30 minutes from 20°C to 30°C. An inverse relationship between the temperature and the wavelength was observed. The total measured wavelength difference was approximately 10 pm to 15 pm.

The polarization variability rate and amplitude of the WR-PTP signals over aerial and underground links were characterized to understand how the differences in environmental conditions can affect polarization stability. A variable coupler was used in the W3-W4 link to take a minimal portion of the WR-PTP signals, to measure the polarization state with a polarimeter while allowing sufficient optical power to maintain lock between the WR nodes to simultaneously measure the clock delay. Fig. 4B and Fig. 4D show the polarization drift and clock delay over 3 days for the W3-W4 link. Polarization drift was measured on two adjacent fibers. There is a clear difference in variations between night and day, for both clock delay and polarization drift. The polarization drift was correlated with thermal and acoustic fiber fluctuations in the aerial link. The W3-W5 (30 km) and W3-W0 (7 km) underground loopback fibers were characterized for approximately one hour starting at noon local time, i.e. during higher temperature gradients. The polarization drift (Fig. 4C) is characterized by the angle variation,  $\delta$ , relative to the initial reference

point on the Poincare sphere (see Supplementary Materials I). The average and maximum polarization angle variation per minute for the aerial link was  $0.75 \text{ rad} \pm 0.45 \text{ rad}$  and 1.34 rad, respectively, while the average and maximum variation of the most stable underground link (W3-W0) was  $0.02 \text{ rad} \pm 0.01 \text{ rad}$  and 0.03 rad, respectively. However, the maximum angle variation was 0.09 rad over the longer underground link (W3-W5).

Variations  $\sim 0.5 \mu$ W was observed at the SFP photodiode over the W0-W1 deployed link (Fig. 4E). Variations  $\sim 0.5 \mu$ W at the SFP photodiode and  $\sim 5 \mu$ W at the SFP laser were also observed over the W3-W4 deployed link. To understand the impact of optical power fluctuations on the clock delay, a controlled experiment with a variable attenuator between the transmit fiber from the SFP and the optical switch over the W4-W3 link was performed. The optical power variation was initially confounded by air temperature changes. Once the outdoor temperature stabilized to within 1°C over several hours and the path delay was relatively stable, a 1 ps change in clock delay per 1 dB of attenuation was observed (Fig. 4F).

To assess the viability of co-existence over the deployed links, the noise profile must be characterized at the single photon level. Scattered light in the fiber was measured with superconducting nanowire single photon detectors (SNSPD) to capture the noise leakage created by the classical signal in the O-band over the C-band spectrum using tunable filters (Fig. 5). Measurements over the deployed link show that for a clean source transmitting a 1 mW classical signal in the O-band, a quantum source signal can co-propagate in the C-band using the same link. For an O-band source 1280 nm and below, a quantum signal at 1550 nm would experience negligible additional noise from the classical source (Figs. 5A,B). However, the SFPs require filtering to suppress the noise from the back scattering in order to co-propagate a quantum signal over the deployed link. The SFP plots without a CWDM in Fig. 5C are comparable, indicating that most of the noise is due to the source. The filters (Fig. 5D) provided nearly an order of magnitude improvement in noise. The measurements show peaks near 1550 nm. The peak is presumed to be the back scatter from the 1270 nm SFP.

In conclusion, we have described the design, implementation, and characterization of a readily scalable synchronization network based on atomic clocks specifically to meet quantum networking research requirements. The TDEV was  $\sim 10^{-12}$  at short time intervals for both solutions with and without active phase stabilization. With active phase stabilization, two links can maintain  $10^{-12}$  over one month. Path delay gradients, strongly correlated with air temperature gradients, remain the dominant source of clock transfer performance degradation. Additional characterization was necessary to understand the parameters necessary to model and compensate for errors from chromatic dispersion, polarization drift, polarization-dependent loss, and optical power fluctuations to further improve the synchronization precision between nodes beyond  $10^{-12}$  TDEV in commercially available optical clock transfer systems. While underground fibers can mitigate the fluctuations induced by air temperature changes, it is also im-

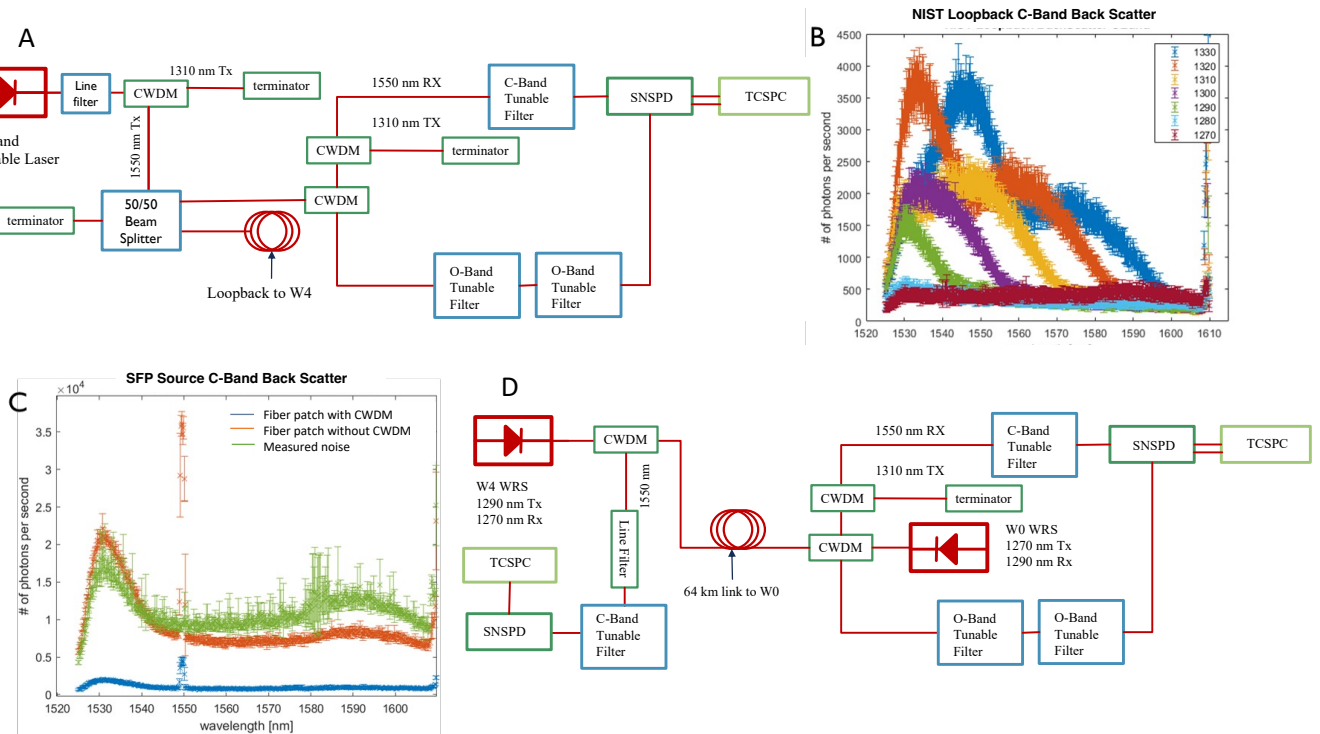


FIG. 5. (A-B) The experimental setup for a clean laser source in the O-band over the 128 km loopback fiber. (C) The noise from the tunable laser (green) and the SFPs (orange) measured directly with only a fiber patch. The blue plot shows the measurement of the SFP with a fiber patch and a CWDM filter. (D) The experimental setup with cascaded O-band tunable filters for 1270 nm and 1290 nm SFP transceivers with a fiber patch cable.

portant for the future robustness, resilience, and scalability of quantum networks to be able to manage and compensate for the phase noise in aerial fibers.

To improve the synchronization precision over deployed fibers for enhancing the performance of quantum network protocols, we have gathered information on various parameters that affect synchronization and plan to build models that will predict the required corrections. The parameters include environmental information such as ambient outside temperature, SFP temperature, and SFP transmitter and receiver optical power that we can sample in real-time.

For future studies, we are pursuing more precise delay information using single-photon measurements such as quantum optical time domain reflectometry. From these models and measurements, we can implement real-time delay corrections in the form of picosecond-level correction values that we believe can be additively combined into a single value. For the WRS, we can dynamically update the asymmetry coefficient used to estimate the one-way delay. The coefficient was originally used to correct wavelength asymmetry due to chromatic dispersion<sup>43</sup> and was a static, calibrated value. A recent enhancement<sup>44</sup> made to the WRS software allows real-time asymmetry coefficient updates. Adjusting the asymmetry coefficient will have the effect of dynamically updating the WRS delay calculation, resulting in a correction to the phase delay of the 1 PPS, 10 MHz, and 62.5 MHz clocks, yielding more precise time synchronization of instrumentation

used in quantum networking experiments. For picosecond-level or better phase stabilization and polarization compensation, co-propagating probe signals at single-photon scales will likely be beneficial. Co-propagating classical probe signals used to compensate for environmental fluctuations can achieve optical frequency transfer on the order of  $10^{-14}$  at 1 s averaging interval using highly correlated adjacent cores in deployed multicore fibers<sup>45</sup>. The bright light from the time synchronization signal requires filtering to reduce light leakage and currently limits the quantum channel coexistence to a separate band. Given the availability of highly-stable atomic clocks and the characterized time transfer capabilities of DC-QNet, the capabilities can be further extended to quantum time synchronization<sup>4,5,46</sup> for secure time transfer.

## I. SUPPLEMENTARY MATERIAL

The supplementary material provides details on the experimental and analysis methodologies.

## II. ACKNOWLEDGEMENTS

We would like to thank all of the reviewers including Jeffrey Sherman and Richard Slonaker for their time and insightful comments.

## III. REFERENCES

- <sup>1</sup>C. H. Bennett and G. Brassard, “Quantum cryptography: Public key distribution and coin tossing,” *Theoretical Computer Science* **560**, 7–11 (2014), *theoretical Aspects of Quantum Cryptography – celebrating 30 years of BB84*.
- <sup>2</sup>C. L. Degen, F. Reinhard, and P. Cappellaro, “Quantum sensing,” *Reviews of modern physics* **89**, 035002 (2017).
- <sup>3</sup>R. Van Meter and S. J. Devitt, “The path to scalable distributed quantum computing,” *Computer* **49**, 31–42 (2016).
- <sup>4</sup>P. Kómár, E. M. Kessler, M. Bishof, L. Jiang, A. S. Sørensen, J. Ye, and M. D. Lukin, “A quantum network of clocks,” *Nature Physics* **10**, 582–587 (2014).
- <sup>5</sup>C. Spiess, S. Töpfer, S. Sharma, A. Kržič, M. Cabrejo-Ponce, U. Chandrashekar, N. L. Döll, D. Rieländer, and F. Steinlechner, “Clock synchronization with correlated photons,” *Physical Review Applied* **19**, 054082 (2023).
- <sup>6</sup>J. S. Bell, “On the Einstein Podolsky Rosen paradox,” *Physica Physique Fizika* **1**, 195 (1964).
- <sup>7</sup>J. I. Cirac, P. Zoller, H. J. Kimble, and H. Mabuchi, “Quantum state transfer and entanglement distribution among distant nodes in a quantum network,” *Phys. Rev. Lett.* **78**, 3221–3224 (1997).
- <sup>8</sup>J. F. Dynes, H. Takesue, Z. L. Yuan, A. W. Sharpe, K. Harada, T. Honjo, H. Kamada, O. Tadanaga, Y. Nishida, M. Asobe, and A. J. Shields, “Efficient entanglement distribution over 200 kilometers,” *Opt. Express* **17**, 11440–11449 (2009).
- <sup>9</sup>J. Yin, Y. Cao, Y.-H. Li, S.-K. Liao, L. Zhang, J.-G. Ren, W.-Q. Cai, W.-Y. Liu, B. Li, H. Dai, G.-B. Li, Q.-M. Lu, Y.-H. Gong, Y. Xu, S.-L. Li, F.-Z. Li, Y.-Y. Yin, Z.-Q. Jiang, M. Li, J.-J. Jia, G. Ren, D. He, Y.-L. Zhou, X.-X. Zhang, N. Wang, X. Chang, Z.-C. Zhu, N.-L. Liu, Y.-A. Chen, C.-Y. Lu, R. Shu, C.-Z. Peng, J.-Y. Wang, and J.-W. Pan, “Satellite-based entanglement distribution over 1200 kilometers,” *Science* **356**, 1140–1144 (2017), <https://www.science.org/doi/pdf/10.1126/science.aan3211>.
- <sup>10</sup>J.-W. Pan, D. Bouwmeester, H. Weinfurter, and A. Zeilinger, “Experimental entanglement swapping: entangling photons that never interacted,” *Physical review letters* **80**, 3891 (1998).
- <sup>11</sup>R. Kaltenbaek, R. Prevedel, M. Aspelmeyer, and A. Zeilinger, “High-fidelity entanglement swapping with fully independent sources,” *Physical Review A* **79**, 040302 (2009).
- <sup>12</sup>F. Samara, N. Maring, A. Martin, A. S. Raja, T. J. Kippenberg, H. Zbinden, and R. Thew, “Entanglement swapping between independent and asynchronous integrated photon-pair sources,” *Quantum Science and Technology* **6**, 045024 (2021).
- <sup>13</sup>T. Gerrits, I. Burenkov, Y.-S. Li-Baboud, A. Rahmouni, D. Anand, O. Slattery, A. Battou, S. Polyakov, *et al.*, “White rabbit-assisted quantum network node synchronization with quantum channel coexistence,” *Conference on Lasers and Electro-Optics* (2022).
- <sup>14</sup>I. A. Burenkov, A. Semionov, Hala, T. Gerrits, A. Rahmouni, D. Anand, Y.-S. Li-Baboud, O. Slattery, A. Battou, and S. V. Polyakov, “Synchronization and coexistence in quantum networks,” *Opt. Express* **31**, 11431–11446 (2023).
- <sup>15</sup>A. Rahmouni, P. Kuo, Y. Li-Baboud, I. Burenkov, Y. Shi, M. Jabir, N. Lal, D. Reddy, M. Merzouki, L. Ma, *et al.*, “Metropolitan-scale entanglement distribution with co existing quantum and classical signals in a single fiber,” *arXiv preprint arXiv:2402.00617* (2024).
- <sup>16</sup>J. M. Thomas, F. I. Yeh, J. H. Chen, J. J. Mambretti, S. J. Kohlert, G. S. Kanter, and P. Kumar, “Quantum teleportation coexisting with conventional classical communications in optical fiber,” *arXiv preprint arXiv:2404.10738* (2024).
- <sup>17</sup>M. Alshowkan, P. G. Evans, B. P. Williams, N. S. V. Rao, C. E. Marvinney, Y.-Y. Pai, B. J. Lawrie, N. A. Peters, and J. M. Lukens, “Advanced architectures for high-performance quantum networking,” *J. Opt. Commun. Netw.* **14**, 493–499 (2022).
- <sup>18</sup>N. Lal, I. A. Burenkov, Y.-S. Li-Baboud, M. V. Jabir, P. S. Kuo, T. Gerrits, O. Slattery, and S. V. Polyakov, “Synchronized source of indistinguishable photons for quantum networks,” *Opt. Express* **32**, 18257–18267 (2024).
- <sup>19</sup>S. R. Jefferts, M. A. Weiss, J. Levine, S. Dilla, E. W. Bell, and T. E. Parker, “Two-way time and frequency transfer using optical fibers,” *IEEE transactions on instrumentation and measurement* **46**, 209–211 (1997).
- <sup>20</sup>J. Ye, J.-L. Peng, R. J. Jones, K. W. Holman, J. L. Hall, D. J. Jones, S. A. Diddams, J. Kitching, S. Bize, J. C. Bergquist, L. W. Hollberg, L. Roberts-son, and L.-S. Ma, “Delivery of high-stability optical and microwave frequency standards over an optical fiber network,” *J. Opt. Soc. Am. B* **20**, 1459–1467 (2003).
- <sup>21</sup>I. Coddington, W. C. Swann, L. Lorini, J. C. Bergquist, Y. Le Coq, C. W. Oates, Q. Quraishi, K. Feder, J. Nicholson, P. S. Westbrook, *et al.*, “Coherent optical link over hundreds of metres and hundreds of terahertz with subfemtosecond timing jitter,” *Nature Photonics* **1**, 283–287 (2007).
- <sup>22</sup>S. M. Foreman, K. W. Holman, D. D. Hudson, D. J. Jones, and J. Ye, “Remote transfer of ultrastable frequency references via fiber networks,” *Review of Scientific Instruments* **78** (2007).
- <sup>23</sup>J. Chung, E. M. Eastman, G. S. Kanter, K. Kapoor, N. Lauk, C. H. Pena, R. K. Plunkett, N. Sinclair, J. M. Thomas, R. Valivarthi, *et al.*, “Design and implementation of the illinois express quantum metropolitan area network,” *IEEE Transactions on Quantum Engineering* **3**, 1–20 (2022).
- <sup>24</sup>J. Serrano, M. Lipinski, T. Wlostowski, E. Gousiou, E. van der Bij, M. Cattin, and G. Daniluk, *The White Rabbit Project* (2013).
- <sup>25</sup>“IEEE standard for a precision clock synchronization protocol for networked measurement and control systems,” *IEEE Std 1588-2019 (Revision of IEEE Std 1588-2008)*, 1–269 (2020).
- <sup>26</sup>J. Savory, J. Sherman, and S. Romisch, “White rabbit-based time distribution at nist,” in *2018 IEEE International Frequency Control Symposium (IFCS)* (IEEE, 2018) pp. 1–5.
- <sup>27</sup>T.-Y. Chen, X. Jiang, S.-B. Tang, L. Zhou, X. Yuan, H. Zhou, J. Wang, Y. Liu, L.-K. Chen, W.-Y. Liu, *et al.*, “Implementation of a 46-node quantum metropolitan area network,” *npj Quantum Information* **7**, 134 (2021).
- <sup>28</sup>M. Alshowkan, B. P. Williams, P. G. Evans, N. S. Rao, E. M. Simmerman, H.-H. Lu, N. B. Lingaraju, A. M. Weiner, C. E. Marvinney, Y.-Y. Pai, *et al.*, “Reconfigurable quantum local area network over deployed fiber,” *PRX Quantum* **2**, 040304 (2021).
- <sup>29</sup>C. Cui, W. Horrocks, L. McCaffrey, V. Nafria, I. B. Djordjevic, and Z. Zhang, “Entanglement distribution and routing in a multi-node quantum network testbed,” in *2021 Conference on Lasers and Electro-Optics (CLEO)* (IEEE, 2021) pp. 1–2.
- <sup>30</sup>M. Pompili, S. L. Hermans, S. Baier, H. K. Beukers, P. C. Humphreys, R. N. Schouten, R. F. Vermeulen, M. J. Tiggeleman, L. dos Santos Martins, B. Dirkse, *et al.*, “Realization of a multinode quantum network of remote solid-state qubits,” *Science* **372**, 259–264 (2021).
- <sup>31</sup>E. Bersin, M. Grein, M. Sutula, R. Murphy, Y. Q. Huan, M. Stevens, A. Suleymanzade, C. Lee, R. Riedinger, D. J. Starling, *et al.*, “Development of a boston-area 50-km fiber quantum network testbed,” *Physical Review Applied* **21**, 014024 (2024).
- <sup>32</sup>T. Lodhen, D. Cottrill, L. Castillo-Veneros, J. Martínez-Rincón, D. Katramatos, P. Stankus, and E. Figueroa, “Towards distribution of memory-compatible polarization entanglement over long distances,” in *Quantum 2.0* (Optica Publishing Group, 2023) pp. QTh2A–40.
- <sup>33</sup>W. McKenzie, Y.-S. Li-Baboud, M. Morris, S. Patel, A. Rahmouni, P. Kuo, O. Slattery, Y. Shi, I. Bhardvaj, I. Burenkov, A. Richards, M. Ayako, B. Crabbill, M. Merzouki, A. Battou, and T. Gerrits, “Towards quantum networking: Characterization of white rabbit precision time protocol over a metropolitan scale fiber link,” in *Precise Time and Time Interval Meeting, Session P3b* (ION, Long Beach, CA, 2024).
- <sup>34</sup>Certain commercial equipment, instruments, or materials are identified in this paper to foster understanding. Such identification does not imply recommendation or endorsement by the National Institute of Standards and Technology, the Department of Defense, or the National Aeronautics and Space Administration, nor does it imply that the materials or equipment identified are necessarily the best available for the purpose.
- <sup>35</sup>L. C. Sinclair, F. R. Giorgetta, W. C. Swann, E. Baumann, I. Coddington, and N. R. Newbury, “Optical phase noise from atmospheric fluctuations and its impact on optical time-frequency transfer,” *Physical Review A* **89**, 023805 (2014).
- <sup>36</sup>J. L. Hanssen, J. A. Taylor, and C. R. Ekstrom, “Time and frequency transfer over an electronically compensated fiber link,” (2013) pp. 235–238.
- <sup>37</sup>P. Krehlik, Ł. Śliwczyński, Ł. Buczek, J. Kołodziej, and M. Lipiński, “ELSTAB—fiber-optic time and frequency distribution technology: A general characterization and fundamental limits,” *IEEE transactions on ultrasonics, ferroelectrics, and frequency control* **63**, 993–1004 (2015).

- <sup>38</sup>M. L. O. Lopez, A. Amy-Klein, “High-resolution microwave frequency dissemination on an 86-km urban optical link,” *Appl. Phys. B* **98**, 723–727 (2010).
- <sup>39</sup>S. Droste, F. Ozimek, T. Udem, K. Predehl, T. W. Hänsch, H. Schnatz, G. Grosche, and R. Holzwarth, “Optical-frequency transfer over a single-span 1840 km fiber link,” *Phys. Rev. Lett.* **111**, 110801 (2013).
- <sup>40</sup>M. Rost, D. Piester, W. Yang, T. Feldmann, T. Wübbena, and A. Bauch, “Time transfer through optical fibres over a distance of 73 km with an uncertainty below 100 ps,” *Metrologia* **49**, 772 (2012).
- <sup>41</sup>P. Koppang, J. Skinner, and D. Johns, “USNO master clock design enhancements,” in *Proceedings of the 38th Annual Precise Time and Time Interval Systems and Applications Meeting* (2006) pp. 185–192.
- <sup>42</sup>S. Peil, T. B. Swanson, J. Hanssen, and J. Taylor, “Microwave-clock timescale with instability on order of  $10^{-17}$ ,” *Metrologia* **54**, 247 (2017).
- <sup>43</sup>P. Jansweijer and H. Peek, “In-situ determination of the fiber delay coefficient in time-dissemination networks,” in *2019 IEEE International Symposium on Precision Clock Synchronization for Measurement, Control, and Communication (ISPCS)* (2019) pp. 1–6.
- <sup>44</sup>Wujek, Adam, Alpha Adjustment Code, [https://ohwr.org/project/ppsi/tree/adam-alpha\\_adjustment](https://ohwr.org/project/ppsi/tree/adam-alpha_adjustment).
- <sup>45</sup>N. Hoghooghi, M. Mazur, N. Fontaine, Y. Liu, T. Hayashi, G. Di Sciullo, D. Ann Shaji, A. Mecozzi, C. Antonelli, and F. Quinlan, “Towards international clock comparisons on a telecom network: ultrastable optical frequency transfer over deployed multi-core fiber,” in *2024 Optical Fiber Communications Conference and Exhibition (OFC)* (2024) pp. 1–3.
- <sup>46</sup>E. S. Polzik and J. Ye, “Entanglement and spin squeezing in a network of distant optical lattice clocks,” *Physical Review A* **93**, 021404 (2016).